Research Article Vol. 3, No. 3 / March 2016 / Optica 339

Role of epsilon-near-zero substrates in the optical response of plasmonic antennas

Jongbum Kim,[1] Aveek Dutta,[1] Gururaj V. Naik,[1] Alexander J. Giles,[2] Francisco J. Bezares,[2] Chase T. Ellis,[2] Joseph G. Tischler,[3] Ahmed M. Mahmoud,[4] Humeyra Caglayan,[5] Orest J. Glembocki,[3] Alexander V. Kildishev,[1] Joshua D. Caldwell,[3] Alexandra Boltasseva,[1] and Nader Engheta[4,*]

[1]School of Electrical and Computer Engineering and Birck Nanotechnology Center, Purdue University, West Lafayette, Indiana 47907, USA
[2]NRC/ASEE, NRL, Washington, DC 20375, USA
[3]Electronic Science & Technology Division, Naval Research Laboratory, Washington, DC 20375, USA
[4]Department of Electrical and Systems Engineering, University of Pennsylvania, Philadelphia, Pennsylvania 19104, USA
[5]Electrical and Electronics Engineering, Abdullah Gul University, Kayseri 38080, Turkey
*Corresponding author: engheta@ee.upenn.edu

Received 19 August 2015; revised 7 February 2016; accepted 9 February 2016 (Doc. ID 246759); published 17 March 2016

Radiation patterns and the resonance wavelength of a plasmonic antenna are significantly influenced by its local environment, particularly its substrate. Here, we experimentally explore the role of dispersive substrates, such as aluminum- or gallium-doped zinc oxide in the near infrared and 4H-silicon carbide in the mid-infrared, upon Au plasmonic antennas, extending from dielectric to metal-like regimes, crossing through epsilon-near-zero (ENZ) conditions. We demonstrate that the vanishing index of refraction within this transition induces a "slowing down" of the rate of spectral shift for the antenna resonance frequency, resulting in an eventual "pinning" of the resonance near the ENZ frequency. This condition corresponds to a strong backward emission with near-constant phase. By comparing heavily doped semiconductors and undoped, polar dielectric substrates with ENZ conditions in the near- and mid-infrared, respectively, we also demonstrate the generality of the phenomenon using both surface plasmon and phonon polaritons, respectively. Furthermore, we also show that the redirected antenna radiation induces a Fano-like interference and an apparent stimulation of optic phonons within SiC.

OCIS codes: (160.3918) Metamaterials; (160.4760) Optical properties; (230.5750) Resonators; (240.6680) Surface plasmons; (250.5403) Plasmonics.

http://dx.doi.org/10.1364/OPTICA.3.000339

1. INTRODUCTION

The field of nanophotonics was initiated with the predominant focus on plasmonic effects in metals, where due to the negative real part of the dielectric function, electromagnetic fields can be confined to subdiffractional dimensions. Since these initial efforts, the field has blossomed to include subwavelength confinement within all-dielectric structures [1–3] and plasmonic/dielectric hybrid metamaterials [4,5], as well as subdiffractional confinement within highly doped semiconductors [6,7], diluted metals [7], two-dimensional (2D) van der Waal's crystals [8–12], and polar dielectric crystals via surface phonon polariton (SPhP) excitations [13–18].

In all cases, materials where negative real permittivity ($\mathrm{Re}(\epsilon) < 0$) is observed also exhibit spectral regions where the real permittivity is positive; hence a cross-over point between these two regimes exists, therefore resulting in an epsilon-near-zero (ENZ) condition at this transition ($\mathrm{Re}(\epsilon) \sim 0$) [19]. This ENZ regime has led to a wealth of predicted novel light–matter interactions [20]. In general, ENZ causes three predominant impacts upon the local electromagnetic fields. First, ENZ materials exhibit an exceptionally high impedance ($Z = \sqrt{\mu/\epsilon}$) mismatch with the surrounding environment, leading to a severely limited penetration and specular reflection of incident fields. Second, the wavelength within an ENZ material will become exceptionally large, approaching infinity, implying that smaller phase variations of the electromagnetic fields should only be observed over the course of many free-space wavelengths [20–24]. Finally, as the index of refraction is directly proportional to the permittivity, $n = \sqrt{(\sqrt{\mathrm{Re}(\epsilon)^2 + \mathrm{Im}(\epsilon)^2} + \mathrm{Re}(\epsilon))/2}$ at optical frequencies, n becomes vanishingly small provided the material is low-loss (e.g., small imaginary part of permittivity [$\mathrm{Im}(\epsilon)$] near the ENZ condition). The first two properties of ENZ materials have been demonstrated within artificial media in the microwave [25] and far infrared and most recently within the visible [26,27] spectral ranges. In addition, strong light coupling to ENZ modes within naturally occurring ENZ materials has been experimentally studied including tunable metamaterials [28], enhanced optical nonlinearity [29,30], ultrafast carrier dynamics [31], thermal emission [32], and perfect absorbers [33,34].

As demonstrated in several experimental studies [28–34], the ENZ response is observed near the plasma frequency of highly doped semiconductors, as well as near the longitudinal optic (LO) phonon frequency of polar dielectrics [18]. Conventional plasmonic materials such as Au and Ag exhibit an ENZ point within the ultraviolet range [18,35,36]; however, optical losses [Im(ϵ)] for these materials are too high to be useful for ENZ-related studies or applications. On the other hand, transparent conducting oxides (TCOs) such as aluminum- or gallium-doped zinc oxide (Al:ZnO or Ga:ZnO) naturally exhibit an ENZ point in the near-infrared range with small Im(ϵ) attributed to the wide bandgap and small Drude damping (γ) [37]. In addition to highly doped semiconductors, polar dielectric and semiconducting materials such as 4H-SiC are also a promising ENZ material in the mid- to far-infrared range. The negative permittivity for polar dielectric materials is derived from polar lattice oscillations within the frequency range between the LO and transverse optic (TO) phonons [18]. Low optical losses are the result of the slow scattering rates of optic phonons, which typically occur on the timescale of picoseconds, in comparison to the faster scattering of free carrier plasmons. In addition, 4H-SiC polytype has a pole in the dielectric functions close to the TO phonon frequency for which the terminology epsilon-near-pole (ENP) [38] has been established. This is to contrast the difference in phenomena between these two conditions. The unique feature of ENP is associated with the highly dispersive dielectric function that results in the extremely large value of permittivity, whereas the ENZ corresponds to exceptionally low permittivity values. The existence of the ENP region in a polar dielectric allows for exploring the fundamentally different physical phenomena in the two types of materials discussed here.

In this work, by employing both TCOs and 4H-SiC as natural, low-loss ENZ materials, we experimentally probe the ENZ effects within simplified systems, as well as provide a platform for manipulating the radiation pattern and spectral response of local optical resonators. A theoretical study of the resonance frequency and electromagnetic field patterns of optical nanoantennas placed on a near-zero index metamaterial substrate was reported in Ref. [39]; however, the practical case of natural plasmonic or polar ENZ substrates and the impact of a vanishing index of refraction upon antenna resonance behavior has not been reported. Through the patterning of periodic arrays of gold antennas upon these materials, we demonstrate the "pinning" of the antenna resonance frequency as a result of the vanishing index of refraction (reduced real permittivity) of the substrate during the spectral approach to the ENZ condition and observe a drastic modification of the associated radiation pattern. Similar behavior was observed near the ENZ and ENP conditions of 4H-SiC. Furthermore, we report on the IR-active LO phonon modes of 4H-SiC demonstrating a Fano-like interference with the antenna resonance that is not observed near the TO phonon nor within the plasmonic response of the TCOs.

2. THEORETICAL STUDY

It is well known that the performance of an antenna is strongly affected by its local environment and the presence of resonant structures and/or materials in its proximity [40–42]. One of the earliest problems of interest in this topic was the development of methodologies and techniques in the design, characterization, and evaluation of radiation and reception of radio-frequency (RF) antennas above the ground soil for radio broadcasting. With recent developments in the field of metamaterials, optical antenna design, particularly for structure-based antennas, has received renewed interest [43].

When an antenna is located at an interface between two dielectric media, e.g., the air–dielectric interface, most of the radiation is directed into the medium with higher relative permittivity, exhibiting a radiation pattern with the main beams directed at an angle related to $\sin^{-1}(n_1/n_2)$ [44], where n_1 and n_2 are the refractive indices of two media with $n_1 > n_2$, and the angle is measured from the normal to the interface. Figure 1(a) sketches an example of such a electric field pattern, emanating from an infinitely long, 2D wire antenna placed on the interface between air and a semi-infinite, loss-less dielectric medium with dielectric constant $\mathrm{Re}(\epsilon) = 2$. In this example, the field pattern is primarily forward-scattered into the dielectric substrate and has two main beams directed at 45 and −45 deg off normal. This feature has been exploited in applications such as subsurface radar imaging and transmission.

When an antenna is placed on top of a low-permittivity ($\mathrm{Re}(\epsilon) < 1$) substrate, the *air* is the "denser" medium with *higher* relative permittivity and therefore the antenna pattern will be predominantly backscattered into the air above (Fig. 1(b)) [45]. We notice that the pattern still has two main beams directed at angles 45 and −45 deg off normal; however, they are now directed into the air. When the substrate is an ENZ material as shown in Fig. 1(c), the resultant beam is directed back towards the normal. However, as the permittivity of the substrate becomes more negative, the electric field generated by this antenna diminishes because the substrate behaves as an electric conductor, shorting out the resonant response as shown in Figs. 1(d) and 1(e). The modification of radiation patterns has been discussed theoretically for artificial ENZ media, such as layered structures and photonic crystals with Dirac dispersion to achieve the effective index of zero near the Dirac point [46,47]; however, to the best of our

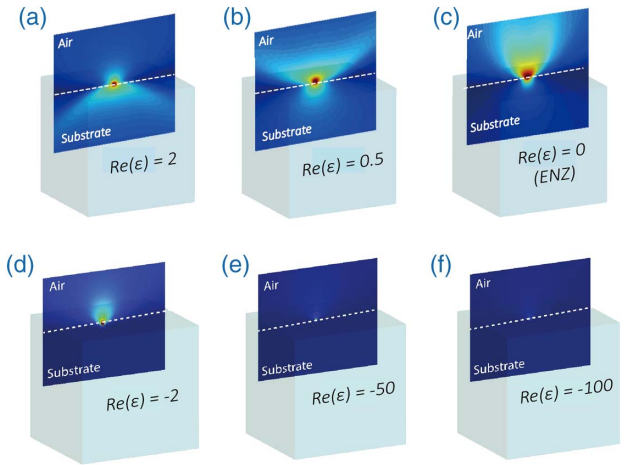

Fig. 1. Electrical field magnitude of a 2D antenna on substrates with different Re(ϵ). The electrical field magnitude pattern of a two-dimensional antenna (infinitely long wire) placed at the interface between air and a semi-infinite (loss-less) dielectric medium with relative dielectric constant of (a) $\mathrm{Re}(\epsilon) = 2$, (b) $\mathrm{Re}(\epsilon) = 0.5$, (c) $\mathrm{Re}(\epsilon) = 10^{-4} \approx 0$, (d) $\mathrm{Re}(\epsilon) = -2$, (e) $\mathrm{Re}(\epsilon) = -50$, and (f) $\mathrm{Re}(\epsilon) = -100$.

knowledge, experimental verification of these predictions on *natural* ENZ substrates has thus far been lacking. (We do note that leaky-wave antennas over bandgap structures with effective index near zero have been demonstrated [46].)

The influence of an ENZ substrate upon the resonance frequency of a local antenna is also of distinct interest if the ENZ phenomenon is to be used for dynamic control of antenna behavior. For any substrate, the antenna radiation may intuitively be assumed as the distribution over two simultaneous paths, one through the substrate and the other through the superstrate, which in this case is air, with the relative efficiencies of these paths defined by the dielectric function of the two local media. The resonance frequency of nanorod antennas has been derived for such systems and can be described as

$$\lambda_{\text{res}} = 2n_{\text{eff}}(L + 2\delta), \tag{1}$$

where L is the nanorod length, δ is the evanescent extension of the resonant antenna mode beyond the physical dimensions of the nanorod, and $L + 2\delta$ accounts for the effective antenna length [41,48,49]. The effective permittivity of the local medium around the antenna can be described as $\epsilon_{\text{eff}} = \frac{\epsilon_{\text{sub}}+\epsilon_{\text{air}}}{2} = \text{Re}(\epsilon_{\text{eff}}) + i\text{Im}(\epsilon_{\text{eff}})$ (assuming an ambient of air, $\epsilon_{\text{Air}} = 1$) [50], where ϵ_{Sub} is the permittivity of the substrate. From the calculated effective permittivity, the effective index can be described as [48,50,51]

$$n_{\text{eff}} = \sqrt{(\sqrt{\text{Re}(\epsilon_{\text{eff}})^2 + \text{Im}(\epsilon_{\text{eff}})^2} + \text{Re}(\epsilon_{\text{eff}}))/2}. \tag{2}$$

For a low-loss substrate, as the effective permittivity of the surrounding medium approaches zero, n_{eff} also becomes vanishingly small. Therefore, in accordance with Eq. (1), due to the high dispersion of the substrate dielectric function near the ENZ frequency, an increase in the antenna length will be compensated by a corresponding decrease in n_{eff}, thereby "slowing down" the spectral shift of resonance frequency near the ENZ condition. This in turn results in the aforementioned resonance "pinning" effect that limits the spectral shifting of the antenna resonance beyond the ENZ condition. Therefore, through the use of ENZ substrates, one can design optical antenna arrays of close arbitrary size/shape within a given range without the antenna dimensions dictating the resonant response. In what follows, we will discuss our experimental results whereby these novel phenomena are experimentally realized and demonstrated within the near- and mid-IR spectral regime.

3. EXPERIMENT RESULTS

The ENZ condition for three material systems (Al:ZnO, Ga:ZnO, and 4H-SiC) of interest in this work is demonstrated in dielectric functions presented in Figs. 2(a) and 2(b), with these materials exhibiting ENZ conditions within the near infrared for TCOs (AZO: 1.29 μm, GZO: 1.19 μm) and mid-infrared for 4H-SiC ($\lambda_{\text{LO}} \sim 10.3$ μm), respectively. In all three cases the substrates can be considered as low-loss, with the $\text{Im}(\epsilon)$ at the ENZ point of Al:ZnO and Ga:ZnO being measured to be 0.29 and 0.31 (Fig. 2(a)), respectively, and for 4H-SiC it can be as low as 0.03 (Fig. 2(b)). As discussed in the previous section, polar dielectric crystals offer natural materials that exhibit ENZ behavior near the LO phonon as well as ENP behavior near the TO phonon ($\omega_{\text{TO}}^{\text{SiC}} \sim 12.5$ μm). This behavior is found within the Reststrahlen band of a polar dielectric or semiconductor material

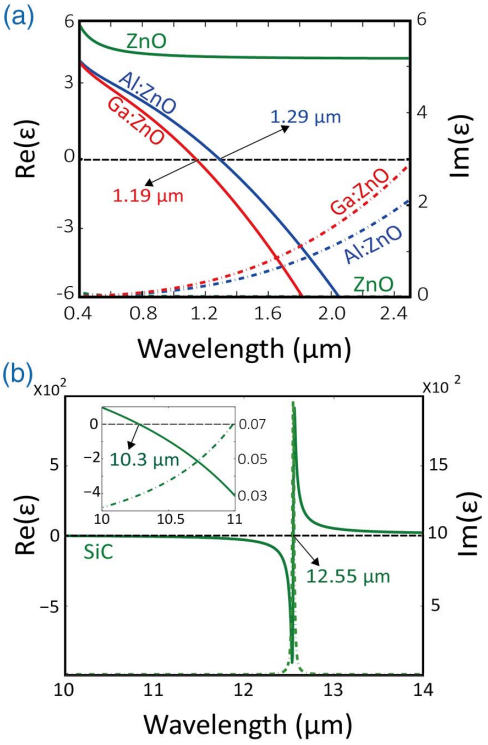

Fig. 2. Optical properties of several ENZ materials. (a) Real (solid lines) and imaginary (dashed lines) parts of the dielectric function of Ga:ZnO (red lines), Al:ZnO (blue lines), and ZnO (green lines). The ENZ points are at 1.19 and 1.29 μm for Ga:ZnO and Al:ZnO, respectively. (b) The SiC dielectric function has the ENZ point at 10.3 μm and an ENP point at 12.55 μm.

that occurs between its LO and TO phonons. In this wavelength range, the dielectric function is negative and light can couple to the LO phonon in much the same way as it does to electrons for wavelengths below the plasma frequency of metals and doped semiconductors.

For probing the impact of the ENZ response upon the local resonant antenna emission, we fabricated a series of rectangular Au nanorod arrays of increasing lengths on these substrates as shown in Figs. 3(a) and 3(b). Since the ENZ frequencies of TCOs and SiC are different, we employed visible and NIR ellipsometry for TCOs and microscope-based Fourier transform infrared (FTIR) spectroscopy for 4H-SiC measurements. The comparison of experimental setups and the general observation of the ENZ impact upon the resonant antenna response will be discussed in following sections.

TCOs (Near Infrared): Periodic arrays of 40-nm-tall and 70-nm-wide Au nanorods of varying lengths were fabricated on a 1.4-μm-thick TCO (Al:ZnO or Ga:ZnO) film deposited on a glass substrate (see Supplement 1). For comparison purposes, Au nanorods were also fabricated on top of undoped zinc oxide (ZnO), which acts as a purely dielectric substrate in the NIR. As shown in Figs. 3(c) and 3(d), the antennas were tilted at 45 deg in reference to the array periodicity so that measurements could be employed to probe the in- and out-of-plane polarization components of the nanorod radiation patterns separately. (See Supplement 1 for additional experimental results from nanorod antenna arrays on TCOs with cross-polarization and copolarization measurement). The resonant excitation of the nanorod will

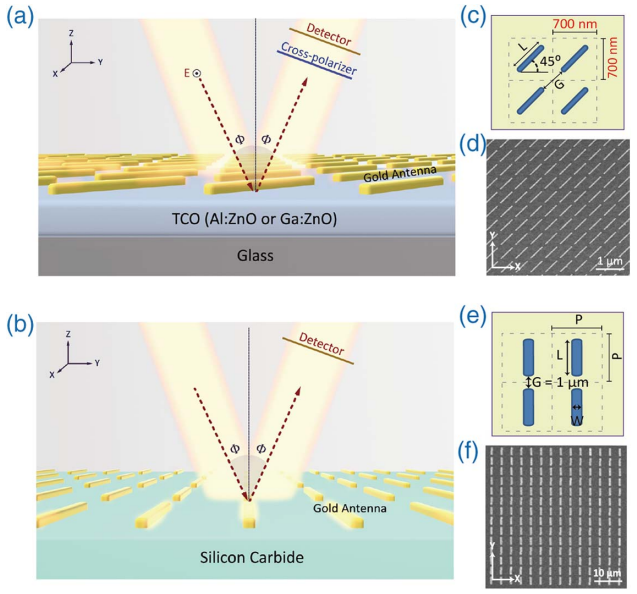

Fig. 3. Schematic of the experimental setup. (a) 45-deg-tilted nanorods are sitting on a TCO layer deposited on a glass. The incident light is directed at the antenna array at an angle of incidence of $\Phi = 20$ deg, and the cross-polarized reflection is detected. (b) In contrast to the Au nanorod antenna array on TCO layers, a nanorod array with rods aligned to the x axis is fabricated on a SiC substrate. Reflection is measured at an angle of incidence of $\Phi \sim 22$ deg. The schematic of dimensions (c) and (e) and the SEM images (d) and (f) of the Au nanorod array on the TCO substrate and on the SiC substrate, respectively, are shown.

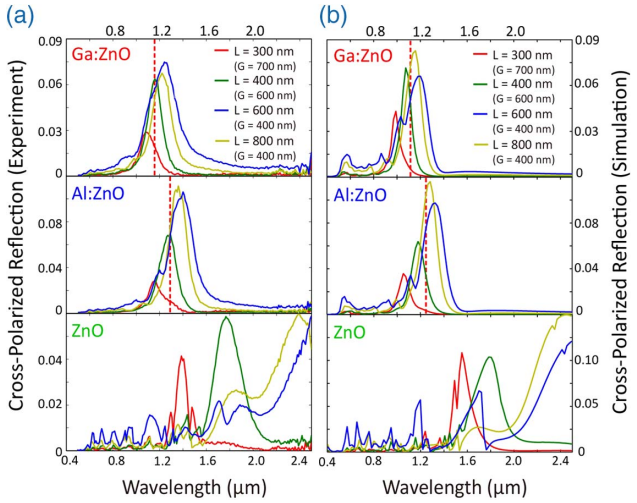

Fig. 4. Optical characterization of nanorod antenna arrays on TCOs. (a) Experimental and (b) simulated cross-polarized reflection spectra of Au nanorod arrays, fabricated on TCOs (Ga:ZnO and Al:ZnO) and dielectric (ZnO) as labeled. Vertical red dashed line indicates the ENZ points for Al:ZnO and Ga:ZnO.

result in a scattering of light with electric field components aligned along both the x and y axes. Therefore, detecting the radiation in the cross-polarized configuration to the incident, only radiation from the antenna with an electric field component along the x axis is measured. The incident light was directed at the sample surface at a 20 deg angle of incidence (Φ), and the reflection spectra were collected in the cross-polarized configuration (Fig. 3(a)).

The corresponding cross-polarized resonance spectra are shown in Fig. 4(a) for Au antennas of 400, 600, and 800 nm lengths on Al:ZnO, Ga:ZnO, and ZnO with a fixed periodicity of 700 nm. Similar to the resonance behavior of plasmonic nanorods on conventional dielectric substrates [40,41,48,51,52], the resonance frequency of the Au nanorods on the undoped ZnO film exhibits only a large spectral red-shift with increasing nanorod length. In contrast, the antenna resonances exhibit a drastically reduced red-shift on the Ga:ZnO and Al:ZnO substrates. In all three cases, the intensity of the reflection is gradually increased as the density of antenna per unit area is increased. (See Supplement 1 for additional experimental results from nanorod antenna arrays on TCOs with fixed gaps between neighboring antennas). In order to explain this small spectral shift of resonance frequency despite the large increment of the antenna length (up to 100% increase), the effective antenna length ($L_{\text{eff}} = L + 2\delta$) as a function of the resonance wavelength (λ_{res}) is provided in Fig. 5(a). The effective length is computed according to the presented equations in the previous section. Since the permittivity of ZnO is almost constant in the measured spectral range, the free-space resonance wavelength of the antennas on ZnO shifts linearly with increasing antenna length. However, the resonance wavelength of the antenna fabricated on the Ga:ZnO and Al:ZnO substrates asymptotically approaches the ENZ frequency of the substrate, and the rate of the resonance shift slows due to the corresponding reduction in n_{eff}. This results in a "pinning" of the resonance near the ENZ condition that can be ascribed to a reduction in n_{eff} that is compensated by a corresponding increase in antenna length.

As described in Eq. (1), the deviation between physical (real) antenna length and calculated effective antenna lengths represents the extension of the resonant mode (2δ) at the nanorod end. From Fig. 5(a), we can extract the value of 2δ by taking the difference between the calculated Leff and the measured L in SEM. It can be seen that the magnitude of 2δ is relatively constant. To add clarity, the near-field distribution around antenna with different lengths placed on either ZnO or Al:ZnO at the corresponding resonance wavelength is depicted in Fig. 5(b). Regardless of the substrate, the dimension of the extended evanescent near field from the end of the nanorod antenna is similar and appears negligible with respect to the physical length.

Silicon Carbide (Mid-Infrared): To explore ENZ effects over a broad spectral range with different material systems and different physical phenomena, we have also employed the polar dielectric material 4H-SiC, as a means of probing this transition. Due to the longer free-space wavelength associated with the ENZ point of 4H-SiC ($\lambda_{\text{ENZ,LO}} \sim 10.3$ μm), Au antennas ranging from 0.5 to 8.4 μm were employed, with the aspect ratio and the edge-to-edge gap between the long axis of the antennas held constant at 4 and 1000 nm, respectively. For the arrays, the periodicity for both axes was equivalent and was designed to be $P_x = P_y = L + 1000$ nm. For comparison to a standard dielectric substrate, a second set of arrays was fabricated on silicon as well. Figure 6(a) depicts the copolarized reflection spectra of the overlying Au antennas on 4H-SiC near the ENZ point. Analogous to the results from the TCOs, as the antenna length is increased, we observe the resonance "pinning" effect as the resonance spectrally approaches the ENZ condition. (See Supplement 1

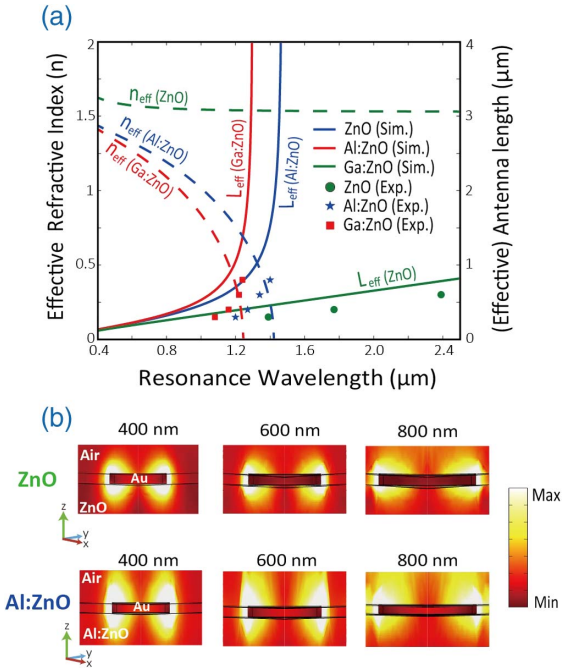

Fig. 5. Analytical characterization of nanorod antenna array on TCOs. (a) Effective refractive index and effective antenna length of nanorod antenna array sitting on Ga:ZnO, Al:ZnO, and ZnO are shown as a function of the resonance wavelength. (b) Simulation results for the norm of local electric fields of nanorod antenna with 400, 600, and 800 nm length on ZnO and Al:ZnO substrate at each resonance wavelength.

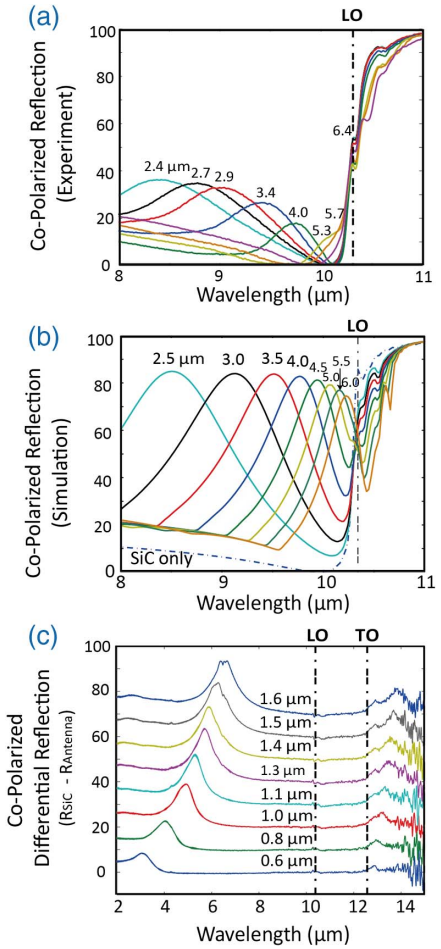

Fig. 6. Structural and optical characterization of nanorod antenna array on 4H-SiC. (a) Copolarized FTIR reflectance spectra for Au antenna arrays of varying lengths on 4H-SiC substrate in the vicinity of the LO phonon wavelength, where the ENZ condition occurs. (b) Simulated spectra for similar antenna lengths to those in (a). (c) Copolarized FTIR differential reflection spectra [R(SiC Only)—R(Antennas)] demonstrating the presence of resonances approaching the ENZ (LO phonon) and ENP (TO phonon) wavelengths of 4H-SiC.

for additional experimental results from nanorod antenna arrays on TCOs with cross-polarization and copolarization measurement). Electromagnetic simulations (Fig. 6(b)) again demonstrate the predominant effect, providing good qualitative agreement with the experimental shifts observed using FTIR reflectance. The factor of two differences in the overall reflection amplitude between the experimental and simulated reflection spectra can be ascribed to increased losses in gold from fabrication, additional resonance broadening due to inhomogeneous structures from lithographic patterning, and imperfect antenna surfaces not depicted in the simulations. In addition to probing the influence of the ENZ substrate upon the antenna resonance, the antenna behavior of the resonance frequency near ENP transition was also investigated. As shown in Fig. 6(c), each antenna actually exhibits two resonances, one to the "blue" (higher frequency) of the LO phonon, while the other occurs to the "red" (lower frequency) of the TO phonon. Much like the case of the ENZ response, a "slowing down" and eventual "pinning" of the antenna resonance is observed; however, this occurs due to the rapidly *increasing* effective index near the TO phonon wavelength that serves to compensate for *reductions* in antenna length. As explained analytically for the TCO systems, the resonance behavior of overlying Au antenna on 4H-SiC and Si substrate can be described by Eq. (1). This can be clearly seen from the plot of the antenna resonance positions with different lengths in Fig. 7(a) with the resonance "pinning" effect resulting in an asymptote at two specific resonance wavelengths $\lambda_{res} \sim \lambda_{ENZ,TO}$ and $\lambda_{ENZ,TO}$, albeit with the asymptotes pointing in opposite directions. It is clearly observed that a reduction (increase) of the effective index of SiC compensates for the increase (decrease) in antenna length near the ENZ (ENP) condition, whereas similar to the case of ZnO, the antennas on Si exhibit a close to linear trend with increasing length (Fig. 7(a)).

Due to the presence of an IR-active absorption at the LO phonon frequency, a Fano-like interference between the discrete Au antenna resonance with the LO phonon continuum is observed as the resonance approaches the ENZ condition and the two optical modes spectrally overlap. This effect is clearly observed in the cross-polarized spectra presented in Fig. 7(b). Such an interference has been reported previously for gold plasmonic split-ring resonators [53] and nanowires [54] on top of thin (3–10 nm) SiO_2 films. However, this interference was not observed near the TO phonon. The interference between the antenna resonance with the LO phonon absorption can be best described as an anticrossing between the modes due to the strong coupling between the excitations. Such a splitting is apparent in the experimental and simulated reflection spectra in Figs. 6(a) and 6(b), respectively, and was first reported in Ref. [53,54]. In addition to this interference, an increase in the amplitude of the LO phonon

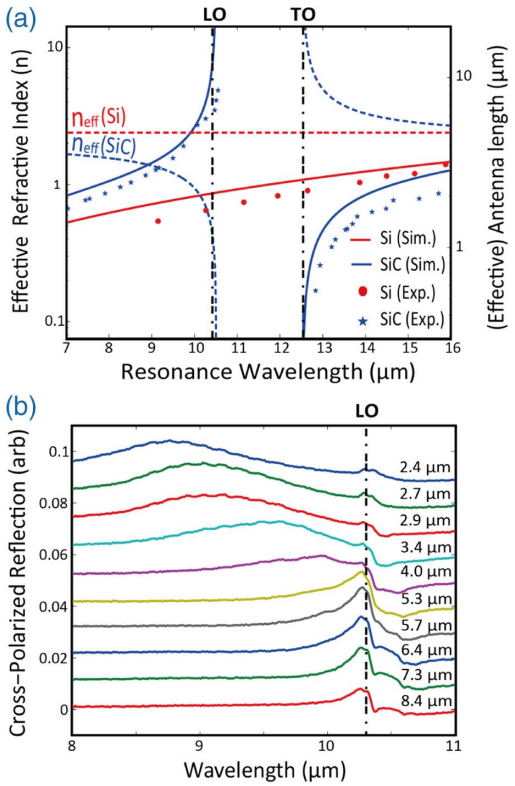

Fig. 7. Analytical characterization of nanorod antenna array on SiC. (a) Calculated effective index (dashed lines, left axis) and effective antenna length (solid lines, right axis) for the antenna arrays on Si (red) and 4H-SiC (blue) substrates. The experimental resonance wavelengths as a function of antenna length are provided as the solid symbols. (b) Cross-polarized FTIR reflection spectra for Au antenna arrays with resonances near the ENZ condition. The Fano-like interference effect and increase in the LO phonon amplitude are maximized when overlap between the antenna resonance and the LO phonon occurs.

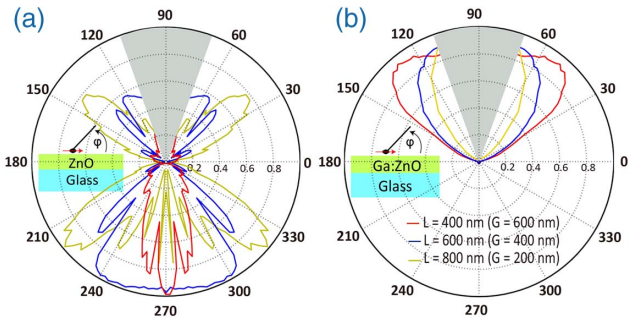

Fig. 8. Radiation patterns of nanorod antenna on ZnO and Ga:ZnO. (a) Radiation pattern of nanorod antennas with three different lengths (400, 600, and 800 nm) on ZnO and (b) on Ga:ZnO substrate at the corresponding resonance wavelength. Sectors with gray color indicate that the radiation pattern cannot be measured at the angle of φ from 70 to 110 deg due to the limitation of ellipsometry.

mode is also observed, reaching a maximum when the two modes are spectrally coincident. This enhancement of the LO phonon is only observed with an incident polarization aligned along the long axis of the antenna and thus implies that the resonant scattered fields from the antennas are more efficiently coupled to the LO phonons. Electromagnetic simulations of such experiments duplicate this Fano-like lineshape and the increasing LO phonon amplitudes under these conditions, clearly illustrating that this is not simply an experimental artifact. To our knowledge, such a phenomenon has not been reported before and may have implications for waveguiding applications and designs.

ENZ Effects upon Radiation Pattern: The radiation pattern of Au antennas on ZnO and Ga:ZnO was measured at the corresponding resonance wavelength using ellipsometery to explore the cross-polarized radiation pattern from the Au antennas on the dielectric and ENZ substrate. The radiation in the presence of the dielectric ZnO substrate is emitted over a large solid angle, with primary beams directed at 45 and –45 deg off normal, being scattered into both the substrate and air, as shown in Fig. 8(a). However, as we theoretically predicted in the field pattern presented in Fig. 1(c), the radiation from the antennas on an ENZ (Ga:ZnO) substrate is mostly backscattered into the ambient (air) as shown in Fig. 8(b). (See Fig. S-1 in Supplement 1 for the simulation of the radiation pattern of the 2D antenna provided in Fig. 1.) As the antenna length is increased, the solid angle of the emitted radiation is reduced because the resonance spectrally approaches the ENZ condition. From this measurement, we verify that the ENZ response can indeed tailor the radiation pattern of local emitters according to its optical properties. Furthermore, the corresponding reduction in n_{sub} *results* in the wavelength within the ENZ material approaching infinity; thus negligible variations in the phase of the electromagnetic fields are observed over distances in excess of several free-space wavelengths. The observed effects hold promise for unprecedented control over the resonance frequency, radiation pattern, and phase of optical antenna emission with less dependence upon the antenna size, thus offering methods for design whereby the size and density of emitters can be decoupled from the resonance properties. In addition, integrating an optical antenna within an ENZ medium provides some degree of control over the directionality and shape of the radiation pattern, placing less importance on changing the geometry or the design of the antenna itself.

4. CONCLUSION

We have demonstrated that drastic modifications to both the resonance frequency and the directionality of the resonant radiation from local dipole emitters occur in the presence of an ENZ substrate. The nanorods on an ENZ substrate were shown to exhibit a reduced spectral shift of the antenna resonance with increasing antenna length near the ENZ condition, resulting in a resonance "pinning," whereby the resonance frequency becomes essentially independent of the antenna length. This was accompanied with a modification in the radiation pattern, with the emission confined to a very small solid angle centered about the normal. A comparison between the resonance behavior of Au nanorod antennas on highly doped TCOs and that on the undoped, polar dielectric 4H-SiC enables the generalization of such a phenomenon over a broad spectral range and between different origins of the ENZ effect. Furthermore, the polar dielectric material system allowed for the investigation of the role of ENP substrates on the antenna resonance, resulting in similar "pinning" behavior, albeit due to a compensation of antenna length *reduction* with rapidly *increasing* real permittivity. In addition, a strong coupling between the Au antenna resonance and the LO phonon absorption at the

ENZ condition resulted in a Fano-like interference between these modes, resulting in an anticrossing behavior. This resulted in the antenna-induced increase in the LO phonon amplitude, which may imply that the antennas are providing scattering-induced enhanced excitation of LO phonons within the 4H-SiC material. These results may provide for possibilities of identifying methods to overcome the geometric dispersion of emitters used in sensors and isolating various plasmonic devices for on-chip nanophotonic devices in flat optics designs and beam-steering applications as well as providing a novel approach to infrared waveguides.

Funding. Office of Naval Research (ONR) (N00014-10-1-0942); Air Force Office of Scientific Research (AFOSR) (FA9550-14-1-0389); NRC/ASEE Postdoctoral Fellowship Naval Research Laboratory Nanoscience Institute (from ONR).

See Supplement 1 for supporting content.

REFERENCES

1. F. J. Bezares, J. P. Long, O. J. Glembocki, J. Guo, R. W. Rendell, R. Kasica, L. Shirey, J. C. Owrutsky, and J. D. Caldwell, "Mie resonance-enhanced light absorption in periodic silicon nanopillar arrays," Opt. Express **21**, 27587–27601 (2013).
2. P. Spinelli, M. A. Verschuuren, and A. Polman, "Broadband omnidirectional antireflection coating based on subwavelength surface Mie resonators," Nat. Commun. **3**, 692 (2012).
3. P. Moitra, Y. Yang, Z. Anderson, I. I. Kravchenko, D. Briggs, and J. Valentine, "Realization of an all-dielectric zero-index optical metamaterial," Nat. Photonics **7**, 791–795 (2013).
4. Z. Jacob, J.-Y. Kim, G. Naik, A. Boltasseva, E. Narimanov, and V. Shalaev, "Engineering photonic density of states using metamaterials," Appl. Phys. B **100**, 215–218 (2010).
5. A. Poddubny, I. Iorsh, P. Belov, and Y. Kivshar, "Hyperbolic metamaterials," Nat. Photonics **7**, 948–957 (2013).
6. A. Boltasseva and H. A. Atwater, "Low-loss plasmonic metamaterials," Science **331**, 290 (2011).
7. G. V. Naik, V. M. Shalaev, and A. Boltasseva, "Alternative plasmonic materials: beyond gold and silver," Adv. Mater. **25**, 3264–3294 (2013).
8. J. Chen, M. Badioli, P. Alonso-Gonzalez, S. Thongrattanasiri, F. Huth, J. Osmond, M. Spasenovic, A. Centeno, A. Pesquera, P. Godignon, A. Z. Elorza, N. Camara, F. J. Garcia de Abajo, R. Hillenbrand, and F. H. L. Koppens, "Optical nano-imaging of gate-tunable graphene plasmons," Nature **487**, 77–81 (2012).
9. S. Dai, Z. Fei, Q. Ma, A. S. Rodin, M. Wagner, A. S. McLeod, M. K. Liu, W. Gannett, W. Regan, M. Thiemens, G. Dominguez, A. H. Castro Neto, A. Zettl, F. Keilmann, P. Jarillo-Herrero, M. M. Fogler, and D. N. Basov, "Tunable phonon polaritons in atomically thin van der Waals crystals of boron nitride," Science **343**, 1125–1129 (2014).
10. Z. Fei, A. S. Rodin, G. O. Andreev, W. Bao, A. S. McLeod, M. Wagner, L. M. Zhang, Z. Zhao, M. Thiemens, G. Dominguez, M. M. Fogler, A. H. Castro Neto, C. N. Lau, F. Keilmann, and D. N. Basov, "Gate-tuning of graphene plasmons revealed by infrared nano-imaging," Nature **487**, 82–85 (2012).
11. A. K. Geim and I. V. Grigorieva, "Van der Waals heterostructures," Nature **499**, 419–425 (2013).
12. J. D. Caldwell, A. V. Kretinin, Y. Chen, V. Giannini, M. M. Fogler, Y. Francescato, C. T. Ellis, J. G. Tischler, C. R. Woods, and A. J. Giles, "Sub-diffractional volume-confined polaritons in the natural hyperbolic material hexagonal boron nitride," Nat. Commun. **5**, 5221 (2014).
13. J. D. Caldwell, O. J. Glembocki, N. Sharac, J. P. Long, J. O. Owrutsky, I. Vurgaftman, J. G. Tischler, F. J. Bezares, V. Wheeler, N. D. Bassim, L. Shirey, Y. Francescato, V. Giannini, and S. A. Maier, "Low-Loss, extreme sub-diffraction photon confinement via silicon carbide surface phonon polariton nanopillar resonators," Nano Lett. **13**, 3690–3697 (2013).
14. R. Hillenbrand, T. Taubner, and F. Keilmann, "Phonon-enhanced light-matter interaction at the nanometre scale," Nature **418**, 159–162 (2002).
15. T. Wang, P. Li, B. Hauer, D. N. Chigrin, and T. Taubner, "Optical properties of single infrared resonant circular microcavities for surface phonon polaritons," Nano Lett. **13**, 5051–5055 (2013).
16. J.-J. Greffet, R. Carminati, K. Joulain, J.-P. Mulet, S. Mainguy, and Y. Chen, "Coherent emission of light by thermal sources," Nature **416**, 61–64 (2002).
17. Y. Chen, Y. Francescato, J. D. Caldwell, V. Giannini, T. W. Maß, O. J. Glembocki, F. J. Bezares, T. Taubner, R. Kasica, and M. Hong, "Spectral tuning of localized surface phonon polariton resonators for low-loss mid-ir applications," ACS Photon. **1**, 718–724 (2014).
18. J. D. Caldwell, L. Lindsay, V. Giannini, I. Vurgaftman, T. L. Reinecke, S. A. Maier, and O. J. Glembocki, "Low-loss, infrared and terahertz nanophotonics using surface phonon polaritons," Nanophotonics **4**, 1 (2014).
19. R. W. Ziolkowski, "Propagation in and scattering from a matched metamaterial having a zero index of refraction," Phys. Rev. E **70**, 046608 (2004).
20. M. G. Silveirinha and N. Engheta, "Tunneling of electromagnetic energy through sub-wavelength channels and bends using epsilon-near-zero (enz) materials," Phys. Rev. Lett. **97**, 157403 (2006).
21. A. Alù, M. G. Silveirinha, A. Salandrino, and N. Engheta, "Epsilon-near-zero metamaterials and electromagnetic sources: tailoring the radiation phase pattern," Phys. Rev. B **75**, 155410 (2007).
22. D. Adams, S. Inampudi, T. Ribaudo, D. Slocum, S. Vangala, N. Kuhta, W. Goodhue, V. Podolskiy, and D. Wasserman, "Funneling light through a subwavelength aperture with epsilon-near-zero materials," Phys. Rev. Lett. **107**, 133901 (2011).
23. B. T. Schwartz and R. Piestun, "Total external reflection from metamaterials with ultralow refractive index," J. Opt. Soc. Am. B **20**, 2448–2453 (2003).
24. E. J. R. Vesseur, T. Coenen, H. Caglayan, N. Engheta, and A. Polman, "Experimental verification of n = 0 structures for visible light," Phys. Rev. Lett. **110**, 013902 (2013).
25. B. Edwards, A. Alù, M. E. Young, M. Silveirinha, and N. Engheta, "Experimental verification of epsilon-near-zero metamaterial coupling and energy squeezing using a microwave waveguide," Phys. Rev. Lett. **100**, 033903 (2008).
26. R. Maas, J. Parsons, N. Engheta, and A. Polman, "Experimental realization of an epsilon near zero metamaterial at visible wavelengths," Nat. Photonics **7**, 907–912 (2013).
27. R. Pollard, A. Murphy, W. Hendren, P. Evans, R. Atkinson, G. Wurtz, A. Zayats, and V. A. Podolskiy, "Optical nonlocalities and additional waves in epsilon-near-zero metamaterials," Phys. Rev. Lett. **102**, 127405 (2009).
28. Y. C. Jun, J. Reno, T. Ribaudo, E. Shaner, J.-J. Greffet, S. Vassant, F. Marquier, M. Sinclair, and I. Brener, "Epsilon-near-zero strong coupling in metamaterial-semiconductor hybrid structures," Nano Lett. **13**, 5391–5396 (2013).
29. A. Capretti, Y. Wang, N. Engheta, and L. Dal Negro, "Enhanced third-harmonic generation in Si-compatible epsilon-near-zero indium tin oxide nanolayers," Opt. Lett. **40**, 1500–1503 (2015).
30. T. S. Luk, D. de Ceglia, S. Liu, G. A. Keeler, R. P. Prasankumar, M. A. Vincenti, M. Scalora, M. B. Sinclair, and S. Campione, "Enhanced third harmonic generation from the epsilon-near-zero modes of ultrathin films," Appl. Phys. Lett. **106**, 151103 (2015).
31. N. Kinsey, C. DeVault, J. Kim, M. Ferrera, V. Shalaev, and A. Boltasseva, "Epsilon-near-zero Al-doped ZnO for ultrafast switching at telecom wavelengths," Optica **2**, 616–622 (2015).
32. Y. C. Jun, T. S. Luk, A. R. Ellis, J. F. Klem, and I. Brener, "Doping-tunable thermal emission from plasmon polaritons in semiconductor epsilon-near-zero thin films,"Appl. Phys. Lett. **105**, 131109 (2014).
33. T. S. Luk, S. Campione, I. Kim, S. Feng, Y. C. Jun, S. Liu, J. B. Wright, I. Brener, P. B. Catrysse, and S. Fan, "Directional perfect absorption using deep subwavelength low-permittivity films," Phys. Rev. B **90**, 085411 (2014).
34. J. Yoon, M. Zhou, M. A. Badsha, T. Y. Kim, Y. C. Jun, and C. K. Hwangbo, "Broadband epsilon-near-zero perfect absorption in the near-infrared," Sci. Rep. **5**, 12788 (2015).
35. P. B. Johnson and R. W. Christy, "Optical constants of the noble metals," Phys. Rev. B **6**, 4370–4379 (1972).
36. E. D. Palik, *Handbook of Optical Constants of Solids* (Academic, 1985).
37. J. Kim, G. V. Naik, A. V. Gavrilenko, K. Dondapati, V. I. Gavrilenko, S. Prokes, O. J. Glembocki, V. M. Shalaev, and A. Boltasseva, "Optical properties of gallium-doped zinc oxide—a low-loss plasmonic material:

first-principles theory and experiment," Phys. Rev. X **3**, 041037 (2013).
38. S. Molesky, C. J. Dewalt, and Z. Jacob, "High temperature epsilon-near-zero and epsilon-near-pole metamaterial emitters for thermophotovoltaics," Opt. Express **21**, A96–A110 (2013).
39. F. J. González and J. Alda, "Spectral response and far-field pattern of a dipole nano-antenna on metamaterial substrates having near-zero and negative indices of refraction," Opt. Commun. **284**, 1429–1434 (2011).
40. R. Adato, A. A. Yanik, J. J. Amsden, D. L. Kaplan, F. G. Omenetto, M. K. Hong, S. Erramilli, and H. Altug, "Ultra-sensitive vibrational spectroscopy of protein monolayers with plasmonic nanoantenna arrays," Proc. Natl. Acad. Sci. USA **106**, 19227–19232 (2009).
41. B. S. Simpkins, J. P. Long, O. J. Glembocki, J. Guo, J. D. Caldwell, and J. C. Owrutsky, "Pitch-dependent resonances and coupling regimes in nanoantenna arrays," Opt. Express **20**, 27725–27739 (2012).
42. R. King and G. Smith, *Antenna in Matter* (MIT, 1981).
43. N. Engheta and R. W. Ziolkowski, *Metamaterials: Physics and Engineering Explorations* (Wiley, 2006).
44. N. Engheta, C. Papas, and C. Elachi, "Radiation patterns of interfacial dipole antennas," Radio Sci. **17**, 1557–1566 (1982).
45. M. Memarian and G. V. Eleftheriades, "Dipole radiation near anisotropic low-permittivity media," Prog. Electromagn. Res. **142**, 437–462 (2013).
46. M. Memarian and G. V. Eleftheriades, "Dirac leaky-wave antennas for continuous beam scanning from photonic crystals," Nat. Commun. **6**, 5855 (2015).
47. M. Memarian and G. V. Eleftheriades, "Light concentration using hetero-junctions of anisotropic low permittivity metamaterials," Light Sci. Appl. **2**, e114 (2013).
48. L. Novotny, "Effective wavelength scaling for optical antennas," Phys. Rev. Lett. **98**, 266802 (2007).
49. T. E. Tiwald, J. A. Woollam, S. Zollner, J. Christiansen, R. Gregory, T. Wetteroth, S. Wilson, and A. R. Powell, "Carrier concentration and lattice absorption in bulk and epitaxial silicon carbide determined using infrared ellipsometry," Phys. Rev. B **60**, 11464–11474 (1999).
50. F. Neubrech, T. Kolb, R. Lovrincic, G. Fahsold, A. Pucci, J. Aizpurua, T. Cornelius, M. Toimil-Molares, R. Neumann, and S. Karim, "Resonances of individual metal nanowires in the infrared," Appl. Phys. Lett. **89**, 253104 (2006).
51. E. Cubukcu and F. Capasso, "Optical nanorod antennas as dispersive 1D Fabry–Perot resonators for surface plasmons," Appl. Phys. Lett. **95**, 201101 (2009).
52. R. Kullock, S. Grafstrom, P. R. Evans, R. J. Pollard, and L. M. Eng, "Metallic nanorod arrays: negative refraction and optical properties explained by retarded dipolar interactions," J. Opt. Soc. Am. B **27**, 1819–1827 (2001).
53. D. J. Shelton, I. Brener, J. C. Ginn, M. B. Sinclair, D. W. Peters, K. R. Coffey, and G. D. Boreman, "Strong coupling between nanoscale metamaterials and phonons," Nano Lett. **11**, 2104–2108 (2011).
54. F. Neubrech, D. Weber, D. Enders, T. Nagao, and A. Pucci, "Antenna sensing of surface phonon polaritons," J. Phys. Chem. C **114**, 7299–7301 (2010).